University of Central Florida

Mechanical, Materials, and Aerospace Engineering

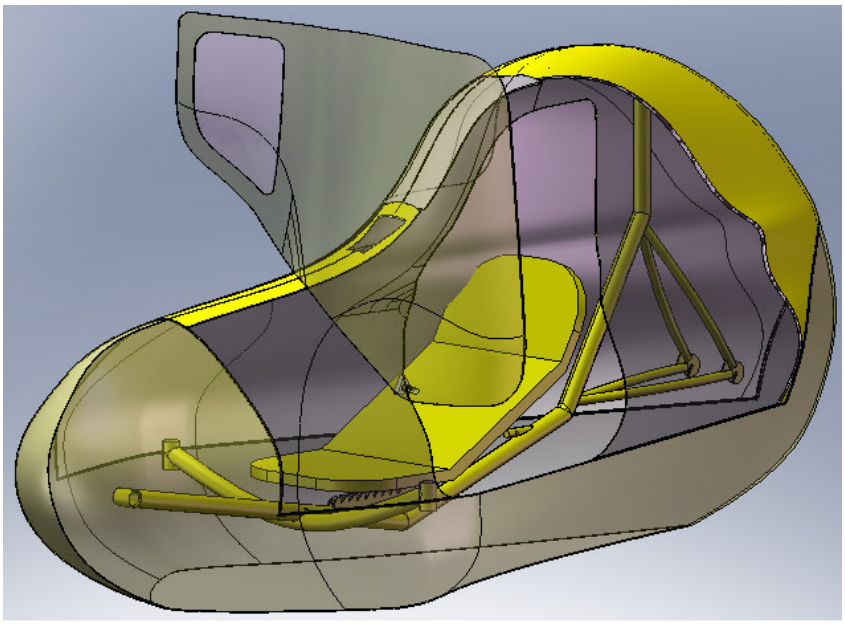

2008 Human Powered Vehicle Challenge
Design Report

Designed By:

Drew Gillespie
Edric Gonzalez
Robert Sheets
Diane Vazquez
Thomas Hardy
Victor Huayamave
Paul Jehlen
Andres Osorio
Luis Rosa

March 22, 2008

Table of Contents

Abstract

Walking, running and swimming are basic forms of human powered transportation that have been available to humanity since ancient times. With the advent of technology, human powered transportation has become more efficient, allowing humans to cover longer distances with less effort. Furthermore, although overshadowed by modern methods of transportation such as cars, airplanes, boats, and trains, human powered vehicles are popular for several motives. Human powered vehicles, such as the bicycle, are low cost, environmentally friendly, and benefit the health of the rider; making them attractive choices for transportation as well as leisure.

In an effort to promote the design, development and exposure of Human Powered Vehicles (HPVs) the American Society of Mechanical Engineers (ASME) sponsors the Human Powered Vehicle Challenge (HPVC). The HPVC challenges Mechanical Engineering students to design and manufacture a HPV that is judged in categories such as overall design, safety and performance. Ultimately, the HPV participates in a competition composed of a time trial and an endurance race against entries from universities across the United States and around the world.

At the University of Central Florida (UCF) participation in the HPVC has become a tradition, and senior Mechanical Engineering students are encouraged to take part in the project. UCF has participated in the HPVC since 2002; in recent history in the East Coast HPVC, the UCF HPV team took 13th place overall in 2005, 6th place overall in 2006, and 3rd place overall place in 2007 in the single rider category. Looking to build on the success the UCF team has had in previous years the 2008 UCF HPV team designed and manufactured an HPV that is a combination of evolution from previous UCF designs and engineering innovation by application of concepts acquired in the classroom.

The 2008 UCF HPV design is an evolution from the 2007 design in multiple aspects. The frame of the HPV retains some features of the 2007 UCF frame such as the tadpole configuration, hydraulic brakes Ackerman steering mechanism, and material selection. Some key differences of the of the 2008 design are the use of a cassette derailleur in substitution of an internal gear hub and an adjustable seat to accommodate for different rider sizes, among other innovations. The most important change in the 2008 frame is the reduction of the overall width of the frame from 33in to 25in, allowing the team to optimize the configuration of the HPV to take advantage of the reduced frame width.

Due to the reduction in the frame width, the team decided to pursue the concept of a fairing that completely enclosed the frame and the rider. As a result, the 2008 UCF HPV has a faring that completely encloses the frame and its occupant. This feature greatly enhances the aerodynamics of the vehicle, ultimately reducing the drag of the vehicle and allowing it to reach speeds greater than a standalone HPV frame. A significant and evident difference between the 2007 and 2008 fairing is the incorporation of a hybrid Carbon-Fiber-Kevlar fabric that allowed for the construction a low weight fairing that reduces the negative effect induced by the additional weight of the fairing.

In general, the 2008 UCF HPV team designed a vehicle that builds on the success of the 2007 HPV. It incorporates successful characteristics observed on previous designs from UCF, while at the same time pursuing innovation and reliability. The report presented in the next pages addresses the methodology, design, and manufacturing processes that the team implemented for the production of the 2008 UCF HPV. The report is broken down into description, analysis, testing and safety sections that address frame and fairing considerations in order to provide a well-rounded perspective of the philosophy taken towards the engineering and construction of the 2008 UCF HPV.

1. Description

The American Society of Mechanical Engineers sponsors the annual Human Powered Vehicle Competition in hopes of finding a design that can be used for everyday activities ranging from commuting to and from work or going to the grocery store. The goals for the University of Central Florida HPV team are to design a vehicle that is lightweight, aerodynamic, safe, and enjoyable to ride, and to be competitive in the 2008 East Coast Human Powered Vehicle Challenge. In the group's endeavor to completely and accurately describe our engineering design problem, a Quality Function Deployment was first performed and a thorough House of Quality was constructed in order to understand the requirements of the project customers, UCF, ASME, SGA, Sponsors, and HPV Riders. The requirements were identified as braking within 20 ft at 15 mph, 100-ft straight steering, 25-ft turning radius, rollover protection, helmet and restraint, no sharp edges, single rider, fast, durable, competitive, comfortable, easy to assemble, lightweight, and cost effective, since budget was $5000.

It was determined that the most important requirements that would give the most advantage in the competition were that it must be fast, competitive, and lightweight. Engineering characteristics, or performance parameters, were then used as quantitative measures to gauge the satisfaction of each requirement and to assure that every requirement issue in the design would be addressed. Upon analysis of this data, it was recognized that the engineering characteristics that have priority in the design are rider change-time less than 15 sec., 50 lb total vehicle weight, 35 inch and 45 inch maximum width and height, 40 mph top speed, and no resonance in steering, seen in Table 1. These are the characteristics that must be optimized in order to meet the most important customer requirements.

Table 1: Target Goals for 2007-08 UCF HPV

Engineering Characteristics	Units	2007-2008 Target	2006-2007 Results
Top Speed	MPH	40	28
Overall Weight	Pounds[lbf]	Under 50	90
Drag Coefficient	Dimensionless	0.2	0.3
Length/Width/Height	Inches[in]	Under 102/33/45	102/33/41
Rider Exchange Time	Seconds[s]	Under 15	22.3
Steering Vibration	--	Null	Present

Benchmark studies were performed on last year's UCF HPV to analyze design strengths and weaknesses and to formulate goals to meet and supercede. This vehicle was a good product to benchmark because it was overall a good design and had good performance. It was discovered that a huge disadvantage of last year's vehicle was its weight. This in turn directly affected the attainable top speed. It also caused problems within the steering, specifically wheel vibration. With this knowledge, the team decided to focus attention on fixing the problems with the vehicle and optimizing all systems and components, gathering information from previous experience and current information on the subject.

The team decided to use the 3-Wheeled Tadpole configuration employed by last year's team because it is inherently stable and makes the learning curve almost non-existent, even for the novice rider. It also reduces the rider change time dramatically since virtually no spotters are needed. The recumbent position provides a comfortable and safe ride due to lower center of gravity which minimizes rollover. The tadpole design makes turning safer, since there are 2 wheels to distribute the navigation of a turn. Rear-wheel-drive is more practical based on the overall vehicle configuration. This year's goal was to optimize every aspect of the vehicle with respect to important variables, which the team determined to be lightweight, maximal speed, minimal frontal area, maneuverability, ergonomics, safety, and reliability.

1.1 Human Fitting and Ergonomics

1.1.1 Wood Mock-up

Upon the creation of a wood mock-up frame the conceptual design was easy to visualize. The frame was constructed and adjusted according to the rider's line of sight and comfort. Blood flow to the rider's legs was taken

into account in the mock-up adjustment to ensure that the work output from the rider was maximized due to low fatigue and optimum circulation. Once the frame adjustments were completed, measurements were taken to find dimensions. A picture of the wood mock-up can be viewed below in Figure 1 along with the dimensions obtained in Figure 2.

Figure 1: Wood Mock-up

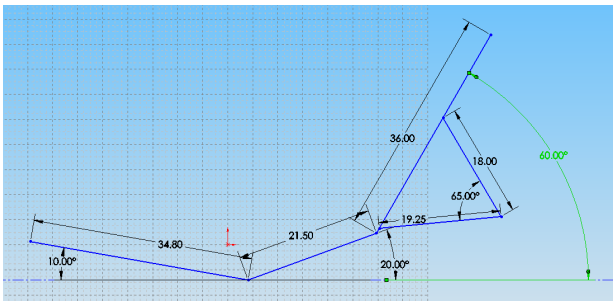

Figure 2: CAD Side View Obtained from Mock-up

1.1.2 Rider Adjustability

Human fitting and ergonomics were investigated with the aid of the wooden mock-up, in order to obtain the best possible configuration that would draw the most power and performance from the rider. The variables that will determine rider comfort are to have at least a ½ inch clearance with the fairing; have strategic positions for the shifter and brakes within 5 inches from the rider's hands; and a comfortable seat with variable adjustment based on rider height. Seat material and adjustment selections were analyzed by weighted rating charts and Carbon Fiber and an adjustable seat were chosen as the best alternatives. Since the UCF HPV team is diverse in height difference, rider height was a key concept that was taken into account. From analyzing last year's adjustable crank boom arm, for a shorter rider, varying the crank distance could shorten the leg distance to the pedals, but would not account for the far distance to the handles. Varying the seat position would account for both of these variables.

Concepts for the adjustable seat were initially sketched as seen in Figure 3, which led to a simple and practical design of a sawtooth plate seat mount, and a sleeve tube that will be welded in through the main tube itself with an inner tube which will slide in and out of the sleeve to allow for adjustability. A feasibility study was done on both mounts to verify that this would work, be safe, and that the dimensions were correct. Two wood sawtooth plates were cut with a jigsaw and were mounted on the wood mock-up, as shown in Figure 4 and dimensions were confirmed. By inspection, it was confirmed that adjustability of the seat would be feasible by hinging the top bracket connection. This was also verified by performing a kinematic simulation in Working Model [1] as illustrated in Figure 5.

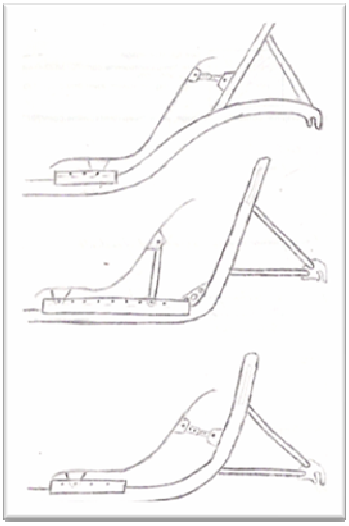

Figure 3: Seat Adjustment Concept Sketches

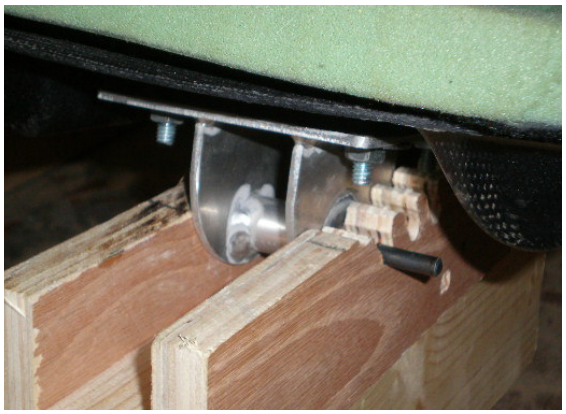

Figure 4: Wood Sawtooth Seat Mount

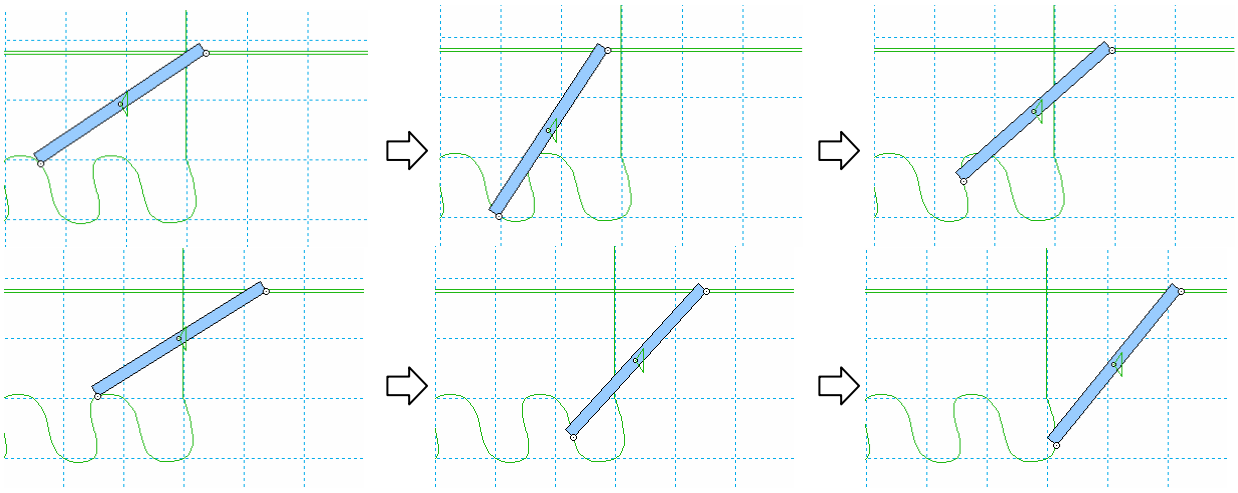

Figure 5: Working Model Illustration of Seat Mechanism Kinematics

1.1.3 Ergonomic Shifter

Ergonomics was kept forefront in mind when deciding what type of shifter to select. In last year's design, a twist-grip shifter was integrated into the handle grip. While sufficient, twist-grip shifters require steering compensation to avoid turning a direct steer trike. To eliminate this problem, it was decided to implement a bar-end shifter instead. This is a better choice and still meets our parameter of having the shifter within 5 inches of the rider's hand.

1.2 Drivetrain

Having an effective drivetrain is a very important factor that will determine the competitiveness of an HPV. The adjustment of gear ratios is what allows the maximum speed to be theoretically achieved by the rider. Weighted rating analysis was done to select the cassette-derailleur system for power transmission to the drive wheel over an internal gear hub. On last year's vehicle, the internal gear hub was implemented, which is comprised of internal planetary gears. A few advantages were that the rider could shift smoothly between gears while stopped, and that the chain did not move sideways when shifting gears. An internal gear hub, however, is considerably heavier than a cassette derailleur system which is used in most bicycle designs. Internal gear hubs are much less efficient than a cassette-derailleur system due to the multiple gear connections which cause more friction and high energy loss. Additionally, a cassette-derailleur is lightweight compared to internal gear hubs and is much less expensive.

Further analysis was done to determine the best combination of crank, chainring, and cassette that will be the best for our top speed goal and also for rider comfort. Since one of the team's goals is to achieve a maximum velocity of 40 mi/hr, an important variable which had to be determined was the size of the chainring. The size of the chainring will determine the maximum speed achievable by the vehicle and is measured by the tooth count around its perimeter. An online velocity calculator [2] was used to determine the maximum speed capable at various chainring sizes with a 10-speed cassette. The results are illustrated in Figure 6.

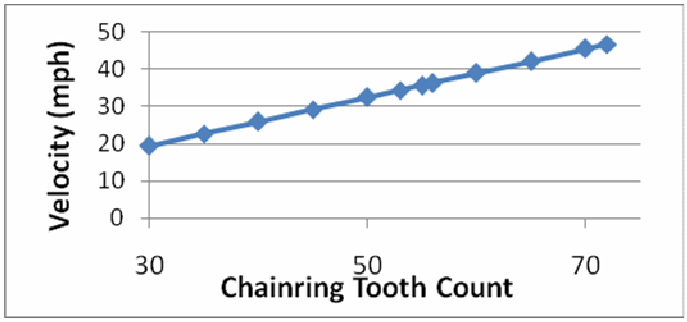

Figure 6: Velocity vs Tooth Count Plot

While a higher tooth count will result in a higher maximum achievable velocity, it will also result in a higher force required to pedal. In this particular case, there are two factors that will determine the size of the chainring. One of these factors is that of the maximum velocity which will act as the lower limit since lower tooth count will result in lower maximum velocities. The other is that of the pedaling force, which will result in the upper limit since the higher the tooth count the harder it is to pedal. Two separate satisfaction curves were generated to evaluate the effects of chainring size based on these factors shown in Figure 7. To obtain the optimum chainring size a weighted satisfaction curve was generated to incorporate both the negative and positive effects of various tooth count, illustrated in Figure 8.

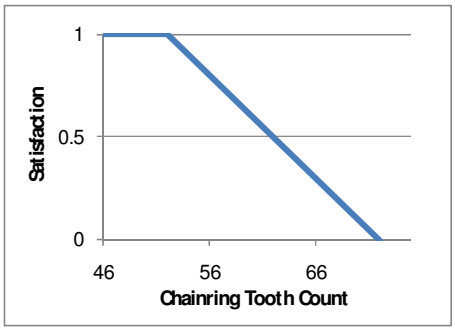

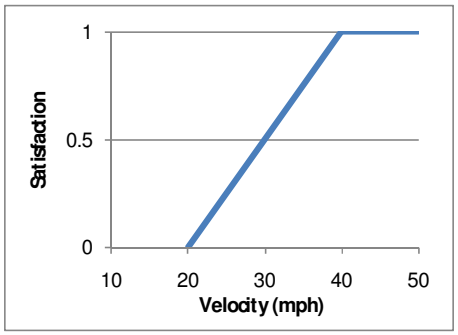

Figure 7a, b: Chainring Size Satisfaction Curves: a) Upper Tooth Count Limit, b) Lower Tooth Count Limit

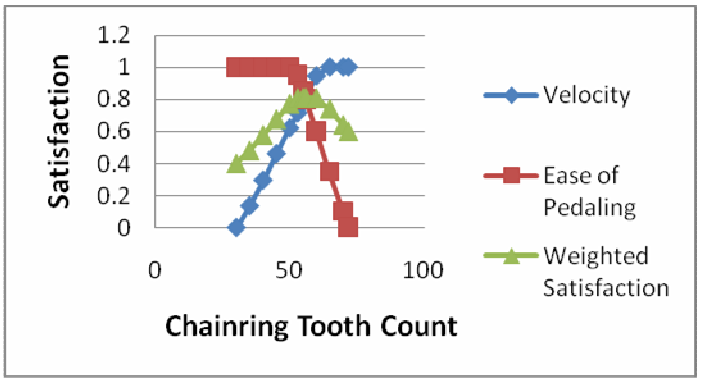

Figure 8: Weighted Satisfaction Curve

The optimum tooth count is determined by that to which corresponds to the highest satisfaction value on the combined satisfaction curve. Therefore, it was determined that the optimum chainring size corresponds to a tooth count of 56. This chainring size will provide the necessary gear ratio with an 11T sprocket to obtain a maximum velocity of 40 mi/hr while still satisfying the pedaling force required by the rider.

Through price-to-weight analysis Table 2 and Table 3 show that based on a budget of $2,500.00 for the frame and an estimated vehicle weight of 35 lbs, the difference in weight does not have a significant effect on the vehicle weight as opposed to the difference in price, which has a significant effect on the budget. A local bike shop, Locomotion [3], was consulted in order to determine the previously quoted prices for various components.

Table 2: Cassette Price-to-Weight Analysis

Cassette 10-Speed 12-27	**Price**	**Weight [g]**
Dura-Ace (Titanium)	$220	194
Shimano 105	$75	256
Difference	$145	62
% of Budget and Vehicle Weight	**5.80%**	**0.39%**

Table 3: Derailleur Price-to-Weight Analysis

Derailleur	Price	Weight [g]
Dura-Ace	$160	180
Shimano 105 – 10 Speed	$70	221
Difference	$90	41
% of Budget and Vehicle Weight	**3.6%**	**0.26%**

From Table 4 [2], it was decided to select a 10-speed cassette simply because of the lower gear ratio change from one speed to another. This will allow the rider to shift gears more efficiently and with less required force.

Table 4: Cassette Speed Analysis

10 SPEED	Low Gear																High Gear
Sprocket Tooth Count	27		24		21		19		17		16		15		14		13		12
Percent Overall Ratio Change		12.5%		14.3%		10.5%		11.8%		6.3%		6.7%		7.1%		7.7%		8.3%	
Average % Ratio Change		**9.5%**																	

7 SPEED													
Sprocket Tooth Count	27		24		21		18		16		14		12
Percent Overall Ratio Change		12.5%		14.3%		16.7%		12.5%		14.3%		16.7%	
Average % Ratio Change		**15%**											

Extensive research was performed in order to determine the crank length. Table 5 illustrates suggested crank length for various rider heights and inseam [4]. This table was used to determine the length of the crank based on the average height based on everyone on the frame and fairing teams. The average height corresponds to crank length of 172.5 mm.

Table 5: Suggested Crank Lengths

Height [ft]	Inseam [cm]	Crank Length [mm]
under than 5'	<= 70	165
5' to 5' 2"	<= 74	170.5
5' 2" to 5' 7"	<= 80	170
5' 7" to 6'	<= 86	172.5
6' to 6'5"	<= 93	175
taller than 6'5"	<= 99	177.7-180

1.3 Braking

Another parameter that must be incorporated in the design is the braking ability. The braking ability is affected by certain variables such as what type of brakes is used, at what velocity the vehicle is going, and the tires used. This will determine if the vehicle will be able to consistently stop within the required distance. Hydraulic Disc Brakes were determined to be the best choice by previous weighted rating analysis over rim cantilever and mechanical disc.

The braking distance of the vehicle must be examined to ensure ASME safety requirements are met. Equation 1 was developed through the work-energy principle, which determines the stopping distance. This

equation depends mostly on the velocity of the vehicle and the coefficient of static friction between the tires and the road.

Equation 1: Stopping Distance Equation

$$D = \frac{V^2}{2\mu g}$$

A satisfaction curve was generated to ensure that the braking distance enforced by ASME is met. The vehicle is required to come to a complete stop within 20 ft when traveling at 15 mi/hr. This requirement may be seen in the satisfaction curve located in Figure 9.

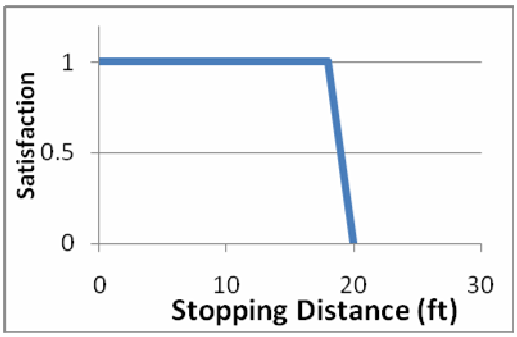

Figure 9: Braking Distance Satisfaction Curve

The stopping distance was determined by using *Equation 1* with a static coefficient of friction of 0.4. Table 1 illustrates the stopping distance at various velocities. When traveling at 15 mi/hr, the stopping distance is approximately 18 ft. It is important to note that a static coefficient of 0.4 is usually characteristic of poor tire conditions. As a result, the stopping distance may be considerably less than that expressed in Table 6.

Table 6: Stopping Distance at Various Velocities

Velocity [mph]	Stopping Distance [ft]
5	2.09
10	8.36
15	18.81
20	33.45
25	52.26
30	75.26
35	102.44
40	133.37

1.4 Steering

Upon research done on previous years' designs, it was noted that a common disadvantage among the past few vehicles was the instability of the steering system. This caused problems such as wheel vibration. Therefore, detailed attention was given to this year's HPV with respect to steering. The integrity of the steering mechanism will directly affect the efficiency of the vehicle since the power generated in the vehicle is transmitted through the tires to the ground. It will also determine the effect of resonance in the wheels, which is a problem that the team aims to resolve from last year's vehicle. Taking these factors into consideration, previous analysis was done to decide which type of steering mechanism would be most beneficial and the best choice. Direct Steering was determined by a weighted rating chart to be the best selection over under seat and above seat steering. With the main dimensions such as wheel track and wheel base, determined from the mock-up, the steering geometry for Ackermann steering, caster angle, and centerline steering were calculated. These factors affect the maneuverability and stability of the vehicle, which is of key importance in the successful design of an HPV.

Ackerman Steering is the adjustment to the direct steering linkage so that the inner wheel will turn at a steeper angle than the outer wheel, depicted in Figure 10. This is a desirable effect in a turn so as to reduce tire scrub, hence increasing efficiency and control in sharp or fast turns. The difference in angle adjusts with the tightness of the turn. This effect is incorporated into the design by angling the tie rod pivots and wheel pivots to intersect with the rear wheel hub, as seen in Figure 11. Calculations were done based on the wheel track and wheel base determined by the mock-up [5], and the Ackerman Compensation Angle was found to be 11.5º.

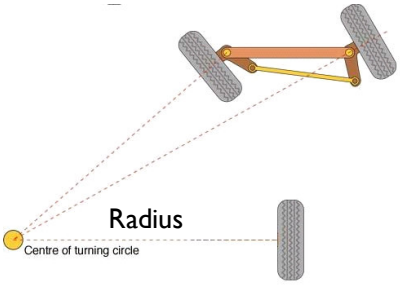

Figure 10: Turning Scenario

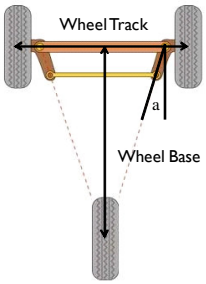

Figure 11: Ackermann Compensation Angle

Another characteristic which should be incorporated into trike steering geometry design is centerline steering. The kingpin angle is associated with this. When centerline steering is implemented, the kingpin axis of a trike meets the ground at or near the contact point of the tire. The kingpin angle of a trike is the angle at which the hub or kingpin is inclined when the wheel is seen normal to the contact patch as shown in Figure 12 [6]. This inclination is used to minimize bump and brake steer by allowing the forces from the impact to be in line with the turning axis. This means that no torque can be exerted that may jerk or bump the steering. Also, uneven braking will not affect the steering with the kingpin inclined. Measurements were taken using an 18" wheel with disc brakes. A kingpin angle of 16.3º was calculated, this was done using the measured dimensions shown in Figure 13.

Figure 12: Trike Kingpin Angle

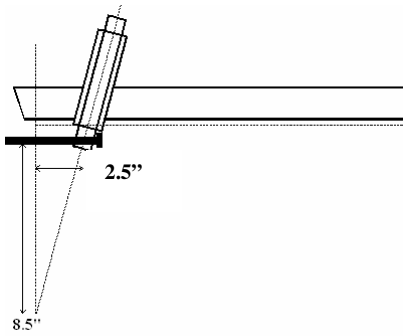

Figure 13: Kingpin Angle Measurements

The last angle of importance associated with frame design is the caster angle. This is the angle of the kingpin when looking normal to the face of the wheel as shown in Figure 14 [7]. This angle controls the trike's ability to self-center. Self-centering is important to trike steering because it makes the trike handle well and remain stable at higher speeds. To achieve self-centering, the kingpin is inclined a second time. This caster inclination occurs in a plane at right angles to the centerline steering angle. A caster angle of 10-14 º is typical on most trikes, and it was decided that 12º caster angle will provide sufficient self-centering, while still being easy enough to turn.

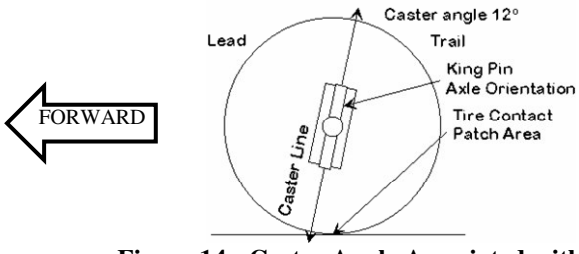

Figure 14: Caster Angle Associated with Frame

1.5 Fairing Design

The 2008 HPV fairing development has taken an evolutionary approach to reach a final design solution. The focus of UCF's 2008 human powered vehicle team is innovation through optimization. Keeping with this theme, the fairing team has placed the most attention on optimizing frontal area (FA), drag coefficient (cD), human fit and weight. To establish a baseline, the 2007 model vehicle was tested where the above parameters in addition to total measured drag were used as comparison metrics.

Two years ago, UCF developed a simple two wheeled recumbent with a fully sealed fairing for the 2006 HPVC, shown in Figure 15. While the frame's steering was "twitchy" and unpredictable, the vehicles fairing exemplified several favorable characteristics:

1. Low Frontal Area – size is only slightly larger than the human rider and vehicle while still keeping large radii curves to prevent disrupting the flow.
2. Easy/Modular assembly – the fairing at a sprint and endurance configuration and the entire frame could be removed with 5 Dzus fasteners.

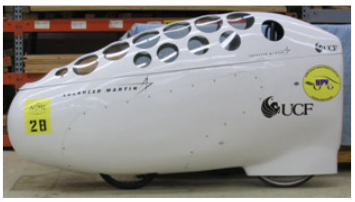

Figure 15: 2006 UCF HPV

Last year, in the 2007 HPVC, UCF competed with a tadpole trike, shown in Figure 16. This solved the instability issues with two wheeled vehicles by providing an inherently safe platform to build upon. Despite this, a traumatic vibration issue was encountered when the fairing was mounted. The fairing had a large frontal area, but accommodated the team's wide variety of body sizes. This problem has since been isolated and resolved and the vehicle made an appearance in the 2007 Maker Faire in San Francisco, California. Faults aside, the fairing has several redeeming characteristics:

1. Rider Cooling – submerged NACA ducts addressed the issue of cooling a human body producing in excess of 1000 watts in a fully enclosed vehicle
2. Excellent visibility – a large windscreen and side mirrors increased vehicle safety
3. Incredibly fast rider exchange – In the endurance competition, the team's best exchange was 14.9 seconds and averaged 22.3 seconds for all four rider changes. This compared to two wheeled competitors taking in excess of 60 seconds to remove and replace the vehicle pilot.

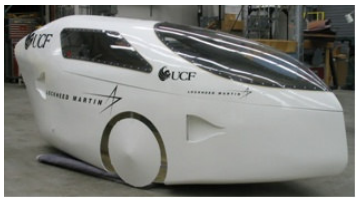

Figure 16: 2007 UCF HPV

In 2008, these concepts met head on. The tight fit of the 2006 model was merged into the safe trike platform of 2007. Frontal Area has been reduced without compromising cD. A windscreen close to the rider's head allows for excellent visibility comparable to the large windscreen (far from the rider's head) on the 2007 vehicle. And finally, an adjustable cooling duct has been employed in the event of a warm or sunny race day in Madison, Wisconsin.

When designing an Aerodynamic feature in an HPV it was clear to the team that a fully enclosed streamlined fairing had to be constructed. The main reason for this is to provide the best aerodynamics achievable, and previous experience has proven this effective. The main characteristic of an aerodynamic shell is to reduce the drag forces created by the vehicle and the air that flows around it when traveling at high speeds. The streamlined body has the lowest of all of the drag coefficients.

The tear drop shape was chosen to be the cross sectional area through all the fairing when viewed from top to bottom. If the fairing is viewed from the side, the shape of the fairing was dictated by giving just enough

clearance to be able to pedal, specifically the crank and knee paths. The shape of the head and rear wheel were also tightened as much as possible.

Although a streamlined body will provide a very small Drag Coefficient, the team had to deal with the actual frame configuration and rider position. To ensure the best shape, the dimensions of all of the persons that could potentially ride the vehicle were taken and used as constrains for the final shape of the fairing. The approach taken was to make the cross sectional area of the fairing as small as possible. To accomplish this, the clearances between the fairing and the frame and rider are very small.

To achieve the best configuration, this year's team looked into their previous fully faired vehicles and decided to redesign and improve from them. Last year's design was fully faired and only the side of the front wheels and a section of the rear wheel were exposed, for this year it was decided that the entire vehicle was to be covered and the wheel areas exposed are going to be minimal. The only areas uncovered are going to be the bottom sections of the wheels that stick out to make contact with the ground.

From research and understanding of the complexity of human powered vehicles or any other aerodynamic machine, the actual aerodynamics only dictates how efficiently the actual power delivery and maximum speed mechanical limitations can achieve. Research studies done by Dr. Joseph Katz from the University of Cambridge show that auto mobiles traveling at speeds over 40mph experience the greatest energy loses due to aerodynamic drag on the body of the vehicle, approximately 60% and 15% for rolling resistance [8]. Therefore, by understanding how fluid over a body acts, it was concluded that by utilizing a streamlined body, a laminar flow can be maintained for longer time at the surface of the fairing and also delaying the development of turbulent flow. This is preferable because when turbulent flow is present, it tends to develop back pressures which relates directly to the increase of drag forces on any type of body.

Table 7 shows the final dimensions of the fairing, and Figure 17 shows the final CAD model of the fairing.

Table 7: Final Fairing Dimensions

Length [in]	98.00
Height [in]	44.50
Width [in]	34.75

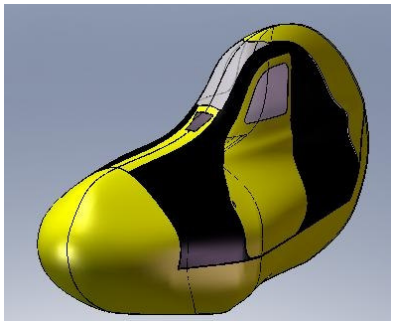

Figure 17: Fairing CAD Model

Another aspect of the final production model is a hinged hatch for easy access in/out for the rider. In conjunction with the three-wheeled design, this will provide a huge advantage during the endurance competition. This concept eliminates the necessity for any other team members to hold the vehicle in the case of coming to a complete stop, for example while the riders change during a pit stop. In addition to functionality of the fairing, aesthetics were also kept in mind since it will influence the overall appearance and public perception of the vehicle.

1.6 Rider Cooling Concepts

An effective cooling system is a very important feature that is also incorporated to this year's HPV; this is a more relevant characteristic during the endurance competition where more heat is emanated by the human body. It was found that the average cyclist could sustain a power output of 0.5Hp (373 Watts) for about 5 to 15 minutes [9]. A human being has an average of 25% for thermal efficiency when in an optimal physical condition; therefore, to calculate the excess heat produced by a person, Equation 2 was utilized. The variables are Q which equals the excess heat, *f* is used as the thermal efficiency leaving P to represent the Power.

Equation 2: Heat Produced by a Person

$$Q = \left[\frac{1-f}{f}\right] \cdot P$$

Due to the results obtained from that equation, 1119 Watts of excess heat is produced while riding, a very efficient cooling system had to be devised to counteract the heat exhaustion that the rider could experience. To achieve the most effective cooling for the rider, several factors were considered. The first and most important is the natural way that the body cools, this way is considered as an evapotranspiration process which uses the own body sweat to cool the rider. Even though the process is effective, it requires air flow over the body and results in fluid losses (sweat). According to the study by Abbot and Wilson, the average fluid losses a rider can experience is a little over 1 liter per hour. The average cruising speed in the endurance race is desired to be 20 – 25 mph for an approximate duration 7- 8 miles per person. Therefore, the average ride time per person for this event is 25 minutes, so each rider could perspire up to 1 liter of fluids during this period of time.

NACA ducts were developed to give a maximum air flow rate while minimizing the drag losses to any type of vehicle. It was obvious that the most optimal place to locate these ducts was in front of the rider in a way to help cool the frontal area of the chest and face and also in the back for the air to exit to ensure that there is flow through the vehicle at all times. The optimal diverging submerged NACA duct is designed with a duct angle between 5° and 7° and a width to depth ratio between 3 and 5 [10]**.** Based on these findings, the ducts will employ a 7° ramp angle with a 3:1 width to depth ratio. Figure 18 shows an example of a NACA duct.

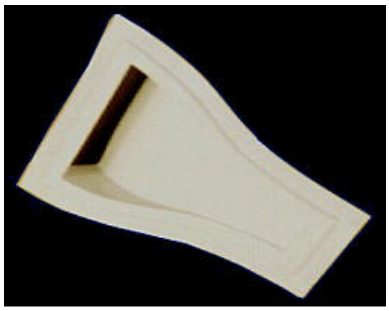

Figure 18: NACA Duct

1.7 Material Analysis

1.7.1 Frame Material Selection

In order to design an effective frame that will function under the prescribed loading conditions and constraints, the best suitable material had to be investigated and selected. Several variables had to be considered such as weight, stiffness, safety, manufacturability, shape factor, and cost. An outcome that must be avoided at all costs is failure by sudden brittle fracture. In the worst case scenario, failure by yielding would be preferred over brittle fracture; this way, failure could be detected before injury could occur. To account for this in the material selection, a fracture toughness of 15 MPa.m$^{1/2}$ was assigned as a design baseline [11], as seen in Figure 19. It is clear that Composites and Metals meet the criteria.

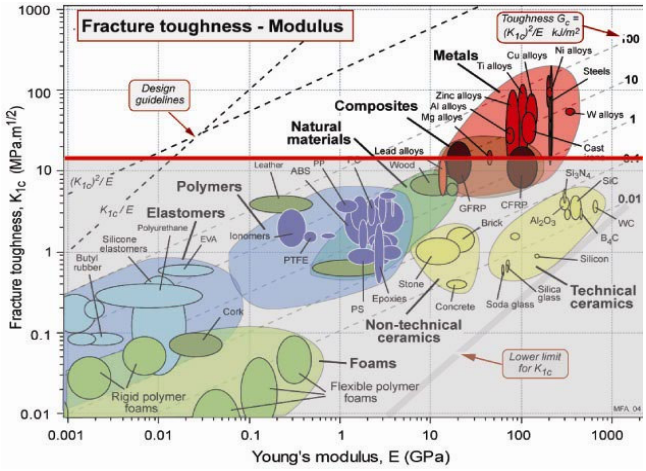

Figure 19: Material Selection Chart - Fracture Toughness

From the two groups, several materials, typically used in this application, were listed to analyze. These include Carbon Fiber, Titanium, Chromoly Steel, and Aluminum Alloys. The selection of the proper alloy of each material was based on the weld-ability of that particular alloy. Their properties and derived shape factor are shown in Table 8 [12]. The shape factor takes into account the material's most efficient manufacturable shape with a limit imposed by local buckling. The objective is to minimize the mass and have a stiff frame that will not deflect under loading. Therefore, several Material Indices were generated (Refer to A6) by which the most appropriate material was selected.

From the stiffness index (Figure 20) it can be seen that all the proposed materials satisfy the stiffness requirements, and that Carbon Fiber would be the best choice, with Aluminum being 2nd best. Applying the shape factor yields similar ranking results (Figure 21). Based on the material properties and shape factor, Carbon Fiber would indeed be the best choice. These however, do not take into account the cost of material, which is a major constraint for our project. Therefore, a third index was generated incorporating the cost per pound of the material. In Figure 22, the Cost Index shows that Steel is the least expensive, with Aluminum coming next. Carbon Fiber is difficult to manufacture to get the desired results, but Steel is much easier to manufacture and machine and still provides safe, excellent results. Titanium is very expensive and has welding limitations. Aluminum is lightweight and affordable, but loses strength dramatically when welded (localized heating), and has to undergo extensive heat treatment.

Given the team's time and budget constraints, this would not be advisable; however, for parts of the frame that require minimal machining and do not experience as much stress, using Aluminum would be advantageous because of its low density. As a result of this analysis, AISI 4130 Chromoly Steel is the best alternative and will be implemented in the main body of the frame, and Aluminum will be used for other small parts, such as tie rods and reinforcement bars. Hence, AISI 4130 will be used for the subsequent frame analysis for this project.

Table 8: Material Properties

Material	Density, ρ [lb/in^3]	Elastic Modulus, E [ksi]	Strength, σ_f [psi]	Stiffness Shape Factor, $(\varphi_B^E)_{max} \approx 2.3\left(\frac{E}{\sigma_f}\right)^{1/2}$	Cost, C_m [US$/lb]
Carbon Fiber (45k filaments)	0.065	32,600	551,000	17.7	8.00
Titanium (6-4)	0.163	15,200	69,600	34.0	26.32
Steel (AISI 4130)	0.284	29,700	63,100	50.0	0.12
Aluminum(6061-T6)	0.0975	10,000	40,000	36.3	1.03
Aluminum(5052-H32)	0.0968	10,200	28,000	43.9	1.03

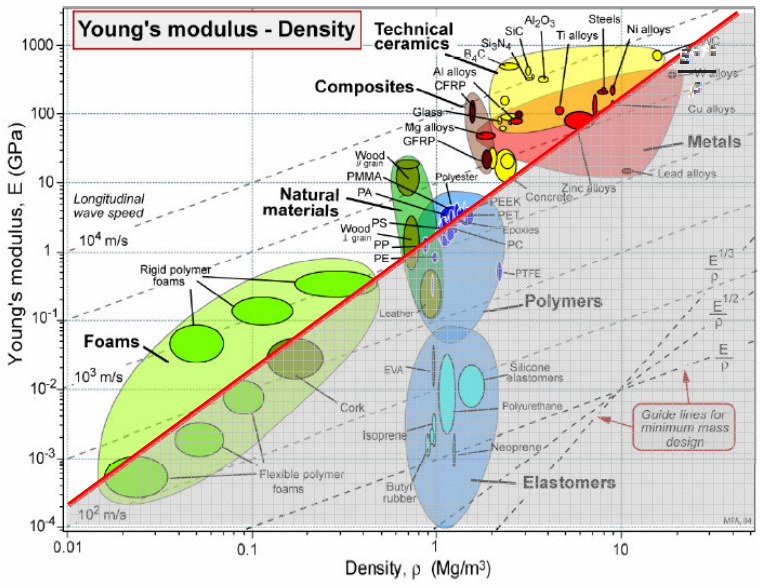

Figure 20: Material Selection Chart - Stiffness Index

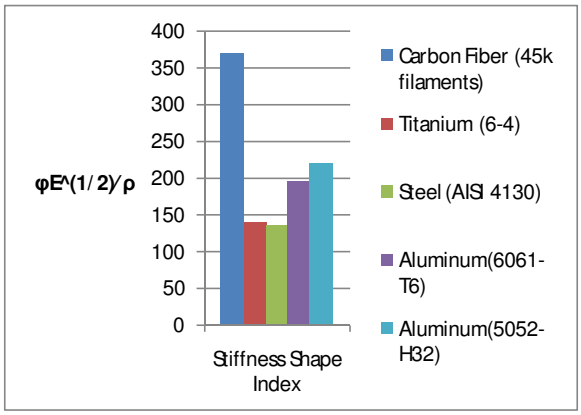

Figure 21: Material Index – Stiffness, Shape

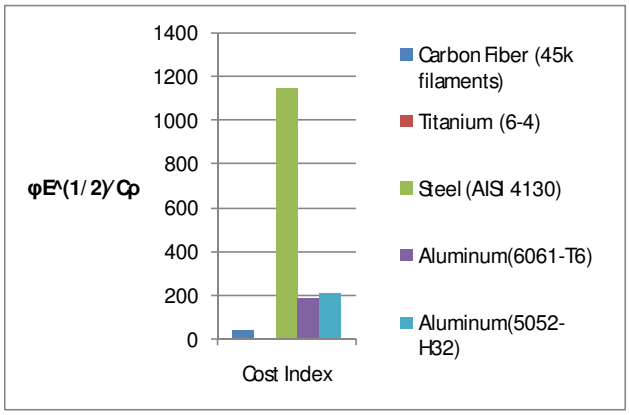

Figure 22: Material Index – Cost

1.7.2 Fairing Material Selection

To obtain optimal performance in the vehicle it is necessary to reduce the weight as much as possible because it doesn't only affect its acceleration for the top sprint competition, it also requires much more energy from the rider to keep the vehicle moving forward at all times for the endurance competition as well. The material that was selected to use for the construction of the Fairing is a Carbon fiber and Kevlar reinforced layer which provides the lightest weight and high strength. This is the most optimum configuration because it not only provides the lighter weight advantage without compromising structural strength, also it is tough enough to withstand a very considerable amount of abuse while maintaining the rider safe at all times (See testing and analysis sections).

1.8 Manufacturing Process

1.8.1 Frame Manufacturing

The manufacturing process for the 2008 UCF HPV is a basic manufacturing process used in many engineering fields today. This first step in any manufacturing process is to create all necessary engineering drawings, as discussed previously. Each individual component needs to have its own drawing with necessary dimensions regardless of how simple the part may be. This is due to the fact that each part will be being made separately. Figure 23 shows the entire assembly for the frame from which individual drawings were taken in order to build the frame to specifications.

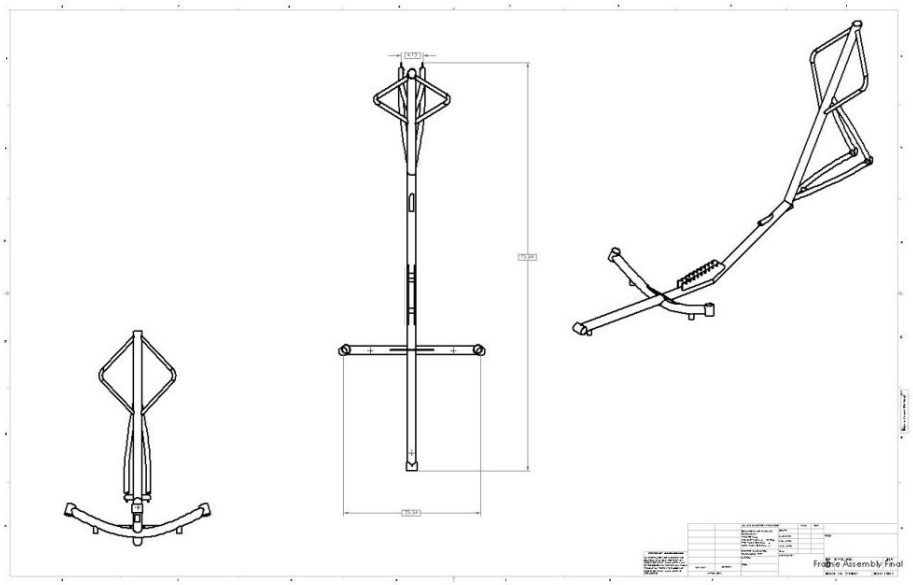

Figure 23: Shows the Engineering Assembly of the 2008 HPV Frame

For the purposes of the HPV construction, the main machining instruments used were a mandrel bender, plasma cutter, manual mill, and a lathe. (See Figure 24 for pictures of manufacturing process.) The main frame pieces (main tube, cross tube and rear stay pieces) were first bent to specification on the mandrel bender. The 1.5 inch outer diameter, 0.049 inch thick Chromoly Steel main tube was then milled at the joints, allowing the separate pieces (crosstube and bottom bracket) to connect seamlessly. One of the most intricate design pieces of the HPV are the sawtooth plates for the seat adjustment, however these pieces were the easiest to manufacture. The plasma cutter was used by uploading the drawing, and the machine automatically cut through 1/16 inch Chromoly plate steel. Gusset plates were also cut in this fashion out of 1/8 inch Chromoly plate steel. Next in the manufacturing process was the assembly of all the pieces.

When integrating all of the individual pieces of the HPV frame welding and bolting pieces were the two main methods used in this process. This step was the most time consuming of the manufacturing processes. The pieces were mounted on a custom made Jig/Fixture. The large flat steel plate (fixture plate) had several custom-made, directionally-isolating fixtures, which were specially made to fit the manufacturing needs. Locating fixtures were placed on the plate and the main tube was tack welded onto the fixtures, as well as the dropout locations. Tack welds were used for all frame-to-fixture connections due to their high strength and ease of removability. The, 1.5 inch outer diameter, 0.065 inch thick crosstube was bent 153º bend and tack welded to the frame. The 2 inch outer diameter headtubes were custom made on the lathe using a boring operation and then tacked onto the crosstube. This was first fastened to the jig with tack welds to ensure correct orientation, then a tig welder using a low-voltage setting was used to rigidly secure the cross tubes to the hubs. The reason why a low voltage was used for the bead weld process is due to the extremely thin tube thicknesses. If too high a voltage were used, the welder would penetrate to deep and deform, vaporize or burn the metal.

The steering tube and the smaller pieces, such as the 0.25 inch outer diameter connection rod, for the steering assembly were machined and mounted into the custom made headtubes, making sure the Ackermann steering angle was taken into account for the correct tierod placement. Next, the 0.058 inch thick, 0.75 inch outer diameter rear stays were fabricated and welded from the frame to the dropouts. Lastly, custom-made seat brackets were made out of Aluminum 6061-T6, to conserve on weight. For the bottom mount, bracket fit right onto the sawtooth plates, and a compression quick release clamp was fastened to it to hold it securely in place. For the top mount, a 0.049 inch thick, 0.75 outer diameter steel sleeve was inserted through the main tube where a hole was drilled. A custom made Aluminum slide tube was cut on the lathe to specs and was hinge fastened to the top bracket. The slide tube was then inserted and compression clamped in the sleeve. After the entire frame was tack welded together, all smaller components were then welded to it and the completed frame was cut from the fixture using a cut off wheel. The remaining procedures were component installation and fairing integration/installation.

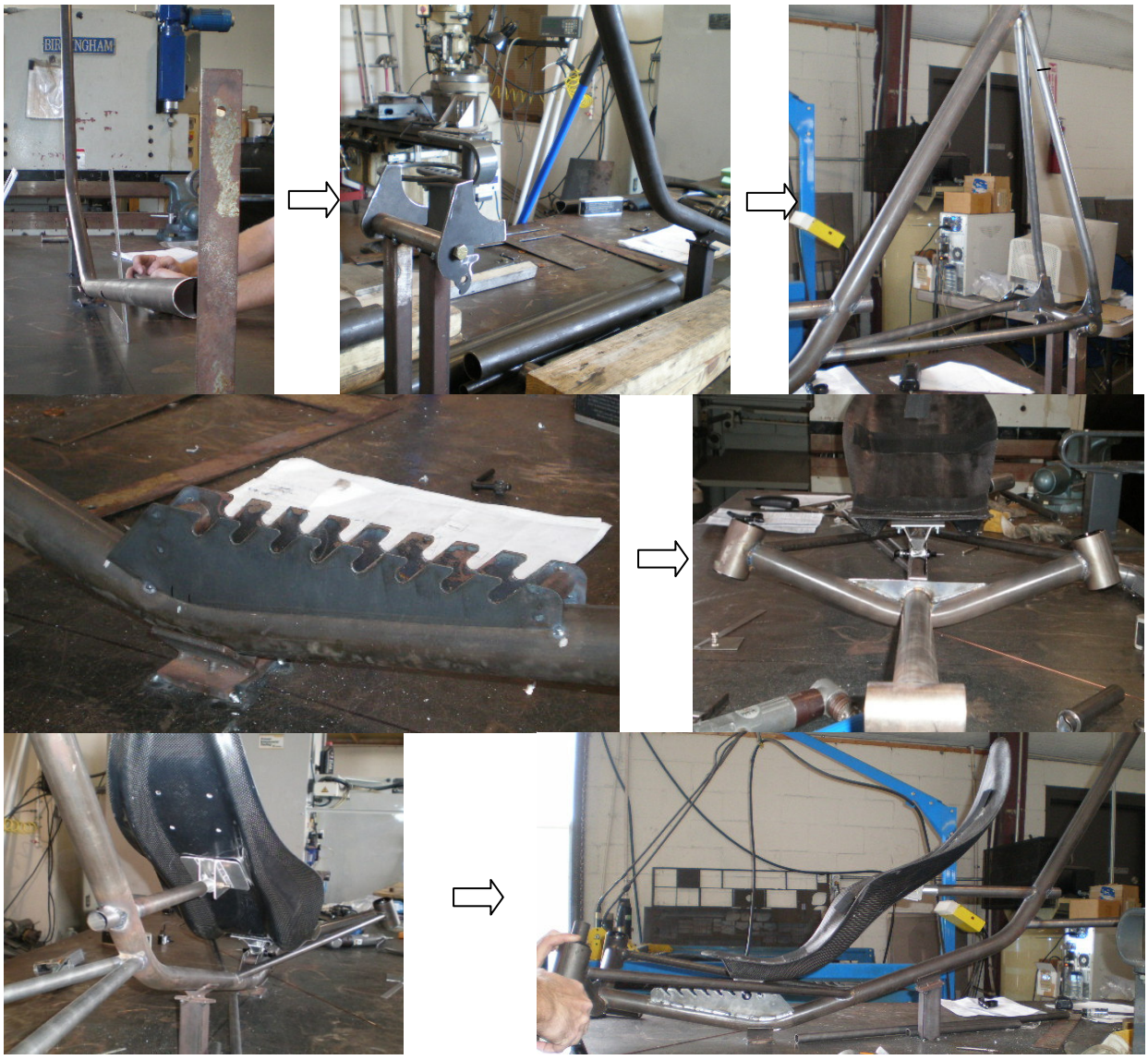

Figure 24: Manufacturing Process for Frame

1.8.2 Fairing Manufacturing

Construction of the fairing is a labor intensive process. First, a foam plug was made, followed by a fiberglass tool that resembles a reversed final shape of the fairing. This tool will be used to vacuum bag the fairing to its final shape.

To build the plug, a solid model was projected onto sheets of foam using a projector and a laptop computer. Using modeled keys of known length, transcription errors were controlled and the team was certain it was tracing at full scale. Cross sections were traced with a marker and later cut out, aligned using PVC pipes, and glued together, as shown in Figure 25.

Figure 25: Initial Stage of Fairing Manufacturing

A conventional cheese grater worked quite well for sanding the foam plug. Unfortunately, polyester resin for fiberglass tooling melts polystyrene foam so a protection layer of joint compound was needed. Also needed was a layer of Bondo to give the plug a smooth surface finish. This took many hours of sanding and patching but it is necessary for a high quality product. A smooth surface is what was modeled and it will produce less drag than a rough surface. Figure 26 shows both the brown Bondo surface and the white wall mud surface.

Figure 26: Fairing Plug

Once the foam plug was deemed acceptably smooth, it was time to construct the fiberglass tool. A table was made and cut out such that the centerline of the plug was coincident with the surface of the table. A layer of wax was applied to the plug and Bondo was used to temporarily seal the plug to the table. This allowed the team to apply fiberglass to exactly one half of the plug and to cast a flange necessary for the vacuum bagging process. Next, the plug and tool were removed form the table, flipped over, and the other half of the tool was laid up. It should be noted that a liberal coat of wax and PVA mold release was used to keep the fiberglass from sticking where it was not desired. Figure 27 shows the assembly of the tool using fiberglass. After curing, excess fiberglass was trimmed off.

Figure 27: Fiberglass Tool

As of this report, the two tools have been removed from the plug and await final lay up. The two halves will be joined, hatches will be cut, and finally the fairing will be joined to the frame.

It should be noted that several test samples were made. A single layer of carbon fiber-Kevlar is flexible and does not hold its shape well. Thus several reinforcement samples were compared. Foam ribs reinforced by fiberglass proved to be extremely lightweight and acceptably strong. Thus they will be used wherever possible to maintain the fairing's shape. Last year's vehicle used Coremat® reinforced with fiberglass. Several test samples of this were tested and proved to be remarkably strong, but were noticeably heavier than the foam even on a one inch by four inch strip. Thus Coremat® will be used where extreme strength is needed, such as structural support ribs.

1.9 Design Innovations

Performance improvement of the frame with regard to last year's results is the main focus of the design objectives for UCF HPV 2008 team. Specific changes were made to optimize performance from the 2007 UCF HPV for this year's HPV race event. The performance design intent takes into account quick rider change and best rider comfort by the implementation of the sawtooth seat mount. The placement of gusset plates bracing the cross tube with the main back bone tube is another innovation incorporated into the frame in order to distribute stress over a greater area, rather than causing stress concentrations at critical points. Improvements on last year's design include using a bar-end shifter instead of a twist grip shifter for easier shifting. Also, a cassette-derailleur is used instead of an internal gear hub for a more efficient and lightweight gearing system.

In the past, vehicles from UCF had used fiberglass fairings, and although fiberglass is a lightweight material there are other available material choices that can significantly reduce the weight of the fairing. In an effort to enhance the performance of the vehicle and reduce its overall weight, the team identified a hybrid Carbon-Fiber-Kevlar weave lighter than fiberglass that still remained a viable option in spite of the limited budget. The 2008 UCF HPV team will be the first in school history to incorporate Carbon Fiber as one of the materials for the fairing, making the 2008 HPV fairing the lightest to date.

In addition, a single pin positioned cleverly will provide a pivot point that allows the hatch to swing up and away from the fairing. This will provide a quick and easy way to enter and exit the vehicle, and it will be lightweight. The pin will be positioned near the front of the hatch. Instead of the rotation axis being normal to the fairing, it will point down slightly. Thus, when it is rotated to lift the door up, the slight downward angle will bring the hatch away from the vehicle, allowing it to swing unobstructed. Figure 28 shows two views of the proposed hatch design in the open position. It should be noted that since this is an exotic design the hatch will be built such that the hinge can be easily swapped to a more conventional design if needed.

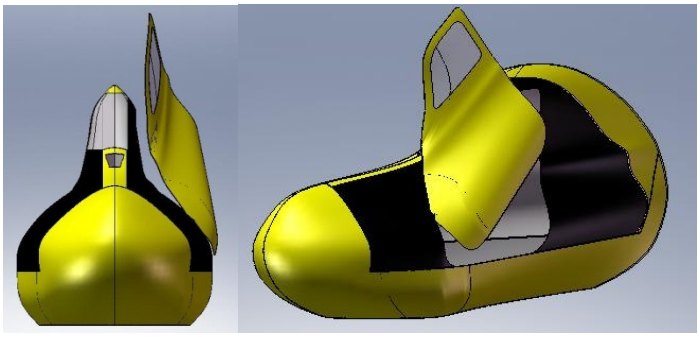

Figure 28: Fairing Hatch Design

2. Analysis

2.1 FEA Analysis

Finite Element Analysis (FEA) was done on the frame to simulate worst-case scenarios, and to analyze the performance of the vehicle in these situations. Several FEA testing analyses were set up to evaluate sound design: rider-loading, rider loading with pedaling, and rider loading with braking, rider loading with torsion. These analyses were done to evaluate the strength of the frame in scenarios that it will experience throughout its life cycle.

The first step in conducting FEA was to set up the mesh using AISI 4130 Chromoly Steel. A shell mesh was the type of mesh used in COSMOSWorks ® within SolidWorks 2007 [13] to simulate the thin piping used in frame design. This is the best type of mesh that could be used because of the nature of the material. A safety factor of 2:1 is considered in all rider loading and road simulation FEA analysis scenarios.

The first of these loading scenarios are a 250-lb rider ranging from the rear seat loading location on the saw-tooth to the front seat location which is used for ease of rider adjustability. Figure 29 displays the deformed view of the static rider loading placed on the 2008 HPV frame. This particular scenario takes into account static rider loading at rear loading location on the saw-tooth mount.

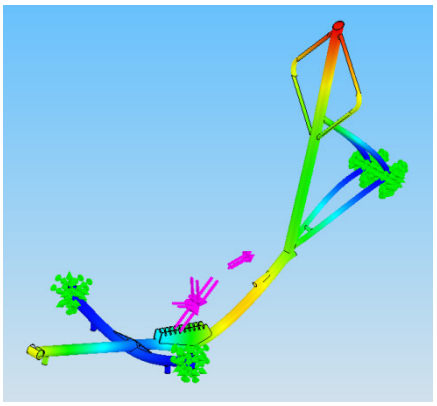

Figure 29: Deformed View Simulating a 250-lb Person

It can be noted that on the back sawtooth position, the frame had a max stress of about 24 kpsi, and on the front tooth the frame max stress was about approximately 15.7 kpsi. The outcome is very acceptable since the stress is well below the Chromoly yield strength which is 63 kpsi.

Next, rider loading with pedaling was simulated in order model a real-world condition that would act on the HPV frame during normal function in a race. A 250-lb rider and a 75-lb pedaling force were placed on the end of the frame where a pedaling torque would act at a 30˚ downward angle. Figure 30 gives the deformed view of the 2008 HPV frame for this scenario, and Table 9 shows the FEA results.

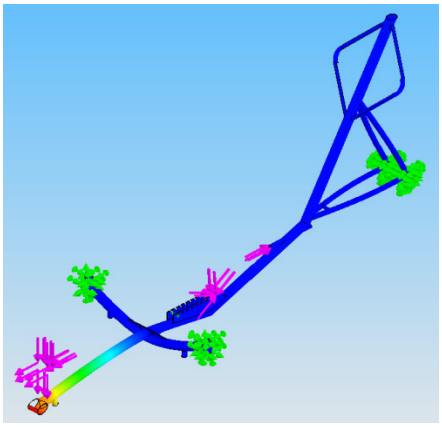

Figure 30: Deformed view Simulating a 250-lb Person and 75-lb Pedaling Torque

Table 9: Analysis Results of Rider Pedaling Scenario

Max Von Mises Stress [kpsi]	73.3399
Max Strain [µin/ µin]	0.00552744
Max Displacement [in]	0.131005

It can be deduced that upon loading of this magnitude, the tubing only strains 0.5 % which accounts for very little plastic deformation. This is acceptable considering the safety factor for the worst-case scenario and the amount of time that the frame will be in actual use for the competition.

The third loading scenario is the rider loading and braking scenario. This scenario takes into account real world braking forces experienced when braking within a 25 ft distance as specified by the rules of this competition. Again a 250-lb load simulating a person was placed on the frame along with a 125-lb braking force. Figure 31 gives the deformed view of the 2008 HPV frame for this scenario, and Table 10 shows the FEA results.

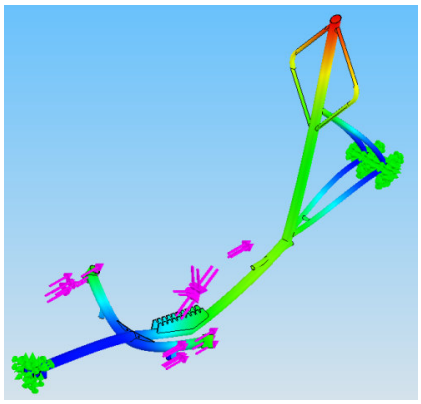

Figure 31: Deformed View Simulating a 250-lb Person and 125-lb Braking Load

Table 10: Analysis Results of Rider Braking Scenario

Max Von Mises Stress [kpsi]	67.1813
Max Strain [µin/ µin]	0.00214436
Max Displacement [in]	0.157203

It can be noted that the strain for the braking simulation was 0.2%, which is still within an acceptable range. This is for a worst-case scenario, so in an average braking situation the vehicle would not experience this deformation.

The fourth scenario of loading conducted on the HPV frame was the torsion scenario. A 250-lb load was placed on the frame to simulate a rider along with a 200-lb torsion force that was placed on the right end of the cross tube. Figure 32 gives the preloaded view and the deformed view of the HPV frame for this scenario. Table 11 displays the results of the torsion scenario.

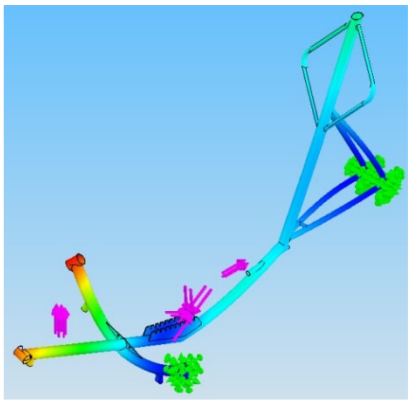

Figure 32: Deformed View Simulating a 250-lb Person and 200-lb Torsion Force

Table 11: Analysis Results of Torsion Scenario

Max Von Mises Stress [kpsi]	47.6523
Max Strain [µin/ µin]	0.00126826
Max Displacement [in]	0.238246

It can be noted that the frame experienced a max stress of approximately 48 kpsi, which is acceptable since the stress is well below the Chromoly yield strength, 63 kpsi.

FEA loading scenarios were carried out to verify and satisfy the ASME guidelines for roll bar safety. As described in the ASME rules, a 485-lb top load and a 260-lb side load loaded independently of each other. Figure 33 gives the deformed view of the frame for and Table 12 displays the results of both roll bar testing scenarios.

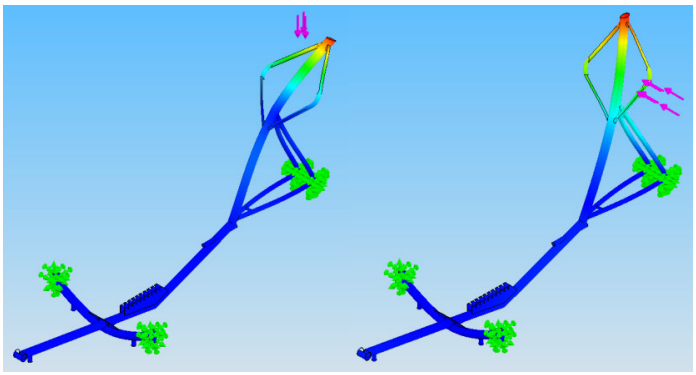

Figure 33: Top and Side Loading on Roll bar

Table 12: Analysis Results for Top and Side Loading on Roll Bar

Top Loading Results	
Max Von Mises Stress [kpsi]	96.162
Max Strain [μin/ μin]	0.00268969
Max Displacement [in]	0.232193
Side Loading Results	
Max Von Mises Stress [kpsi]	42.565
Max Strain [μin/ μin]	0.00169274
Max Displacement [in]	0.241954

Both of the simulated roll bar test scenarios conducted operate well within the specified parameters that the ASME rules stipulate. All of the tests conducted give positive results that point to a sound design. This important because upon manufacturing and testing of the modeled frame this data will help the 2008 UCF HPV team meet its goal to win the competition.

2.2 CFD Analysis

Computational Fluid Dynamics (CFD) is a method to conduct research in the field of fluid mechanics by numerically solving the Navier-Stokes equations using computers. CFD analyses are commonly used for the study of aerodynamics because they present many advantages to the designers. For example they allow the evaluation of the performance of a part, or a design without building a physical model. Moreover, CFD is a very cost effective technique and makes possible to test variations or revisions of a part in a rapid and cost-effective manner.

During the design process of the fairing, CFD was used to evaluate the effectiveness of the fairing and identify areas where improvements could be made. The commercially available code Fluent 6.2 was used to conduct the CFD analyses of the fairing throughout the design process of the fairing. For the CFD model a grid consisting of 1220305 tetrahedral elements was constructed in Gambit 3.2 using a control volume of 24 ft. wide by 24 ft. tall and 48 ft. deep, Figure 34 shows the grid used for all of the CFD analyses.

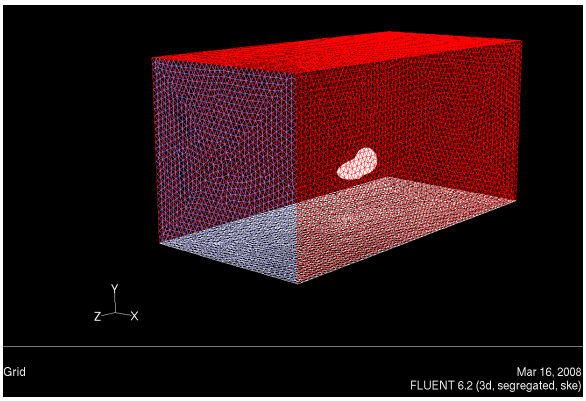

Figure 34: Grid used for CFD Analyses

In addition to solving the Navier-Stokes equations presented in Equation 3, the model that was developed for the CFD analyses used the standard k-ε turbulence model to simulate turbulence effects. In brief, the CFD developed for the study of flow behavior around the fairing consisted of a 3-D steady state simulation, using the standard k-ε turbulence model assuming the flow enters the control volume with a 10% turbulent intensity. The CFD models were run on a UNIX cluster taking advantage of parallel computing in order to reduce computational times.

Equation 3: Navier-Stokes Equation in Vector Formulation

$$\rho\left(\frac{\partial \mathbf{u}}{\partial t}+\mathbf{u}\cdot\nabla\mathbf{u}\right)=-\nabla p+\mu\nabla^2\mathbf{u}+\mathbf{f}$$

A total of three models were developed and solved in order to study the performance of the fairing. The three models created correspond to a low speed scenario, intermediate speed, and high speed scenario; corresponding to 20 miles per hour (MPH), 30 MPH, and 40 MPH, respectively. The results obtained for the three cases are tabulated in Table 13.

Table 13: CFD Results Obtained from Fluent Model

Speed [ft/s]	Area [ft^2]	Pressure Force [lbf]	Viscous Force [lbf]	Total Force [lbf]	Drag Coefficient
29.327	7.824	0.473	0.235	0.708	0.088
43.991	7.824	1.048	0.505	1.553	0.086
58.654	7.824	1.970	0.829	2.799	0.087

The results for the three scenarios show that the vehicle has an average drag coefficient of 0.087, which was calculated using Equation 4 assuming an air density of 0.0023 lbm/ft^3. At 20 MPH the total drag force experienced by the fairing is 0.708lbf, increasing to 1.553 lbf at 30 MPH, and peaking at 2.799 lbf for the 40 MPH situation. Figure 35 presents a plot of the total, pressure and viscous drag forces experienced by the fairing. The total and pressure drag forces have a quadratic behavior, while the viscous force was a linear relationship.

Equation 4: Drag Force Equation used to Solve for the Drag Coefficient

$$F_D=\frac{1}{2}C_d\rho A V^2$$

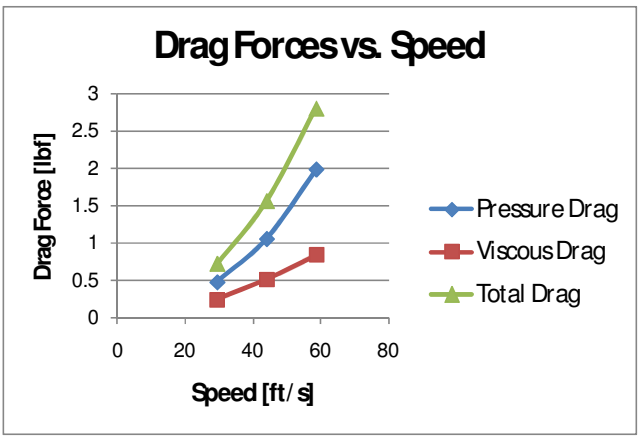

Figure 35: Drag Forces vs. Speed Plot

The low drag coefficient predicted by Fluent is mainly attributed to the low speed of the flow, which translates into a low Reynolds number. Having a low Reynolds number implies that the flow is mainly laminar and that it will remain attached to a surface. Figure 36 shows the contours of local Reynolds number for the 40MPH case. The peak value corresponds to 184, much less that the critical Reynolds number for external flow which is $1x10^5$.

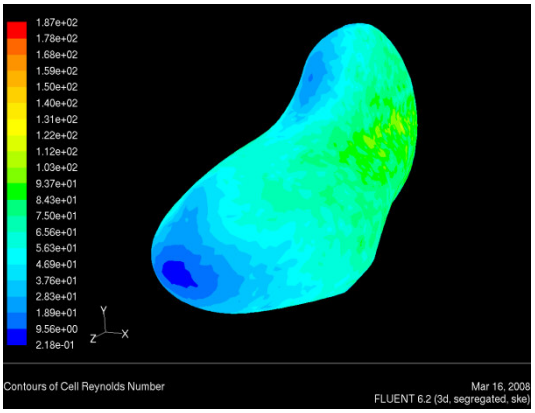

Figure 36: Contours of Local Reynolds Number at 40 MPH

From the results predicted by Fluent it was clearly evident that the entire flow around the fairing was inside the laminar regime. And that the flow would remain attached to the surface of the fairing from the nose until the trailing edge as Figure 37 shows. Similarly, Figure 38 shows the lack of recirculation in the vicinity of the fairing and that the flow remains attached to the surface of the fairing over its entire surface.

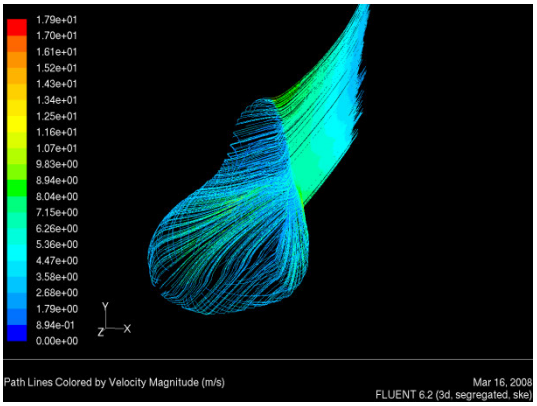

Figure 37: Pathlines at 40 MPH

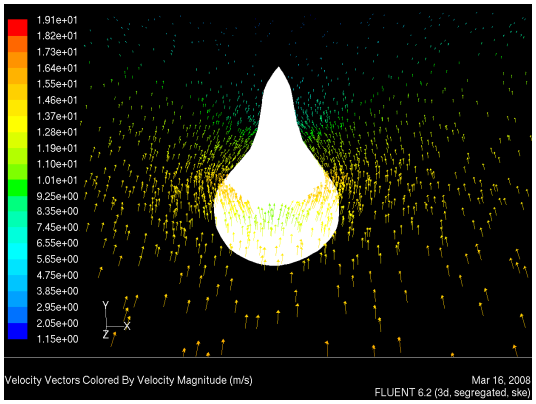

Figure 38: Velocity Vector of Flow Around the Fairing at 40 MPH

Another factor that led to the low value for the drag coefficient is the pressure distribution experienced by the fairing as it is in contact with the flow. As Figure 39 shows there is a concentration of high pressure around the front section of the fairing that is a caused by air being stagnated in the front lower section of the fairing. The next area where there is an accumulation of pressure corresponds to the section covering the shoulders and head of the rider, however not to the extent of the front nose.

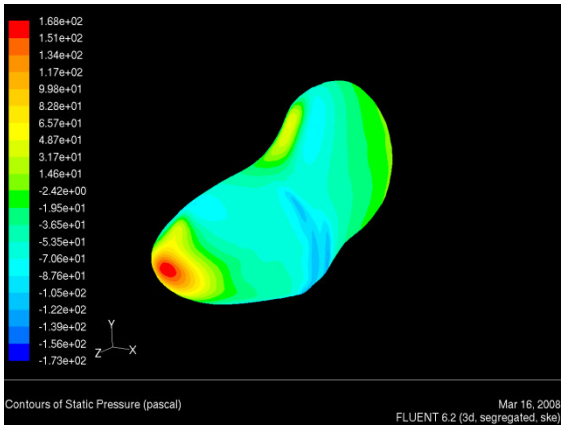

Figure 39: Pressure Distribution along the Fairing Surface at 40 MPH

In summary, the combination of laminar flow and a favorable pressure distribution results obtained by using CFD predict that the drag coefficient of the fairing is 0.087, and that for the expected speeds during the competition the fairing significantly enhances the performance of the HPV. Nevertheless, the results obtained from the CFD models will be compared to physical testing that will be conducted to validate the accuracy of the CFD analyses.

2.3 Economic Summary

One of the most important factors in the design of the vehicle is the restraint caused by the budget. A budget of $5000 was given by the university to provide for materials, manufacturing, and components. Design decisions were based on this budget, and to evenly distribute it, half was given to the frame and fairing teams. Table 14 shows the actual production cost for the 2008 UCF HPV. The total cost for the vehicle is $5230.88. The total cost of the vehicle exceeds the team's budget; however the team was able to assemble the vehicle from donated, inherited and off the shelf parts.

Table 14: Human Powered Vehicle Production Cost

Frame	**Cost**	**Fairing**	**Cost**
Drive Train	$770.00	Resins	$506.25
Tires and Tubes	$91.95	Fabric	$1032.00
Steering	$162.27	Foam	$632.28
Brakes	$275.00	Other	$216.93
Pedals and Shoes	$237.97	Bag Supplies	$236.20
Materials and Labor	$850.00	Adhesives	$65.58
Other	$49.99	Protection	$25.92
Frame Total	**$2437.18**	Sand Paper	$33.89
		Build Frame	$44.65
		Fairing Total	**$2793.70**
UCF Human Powered Vehicle Total Production Cost			**$5230.88**

Production of the vehicle's fairing has a high start up and tooling cost of approximately $1300. These startup costs do not take into consideration major equipment such as a vacuum pump, compressor, major safety equipment and the work space necessary for production. The primary expense for each fairing is the carbon/Kevlar fabric used. If fiberglass at approximately $100 per fairing were used, the production of 120 fairings would cost

$426.29 each. As presented in competition, the cost of the fairing totals $2793.70 which includes the cost of leftover materials; the cost for 1 fairing with no leftover material would be $2159.51. Table 15 shows the vehicle cost for a streamlined production run. Processing includes wet lay up and vacuum bagging. This means both the fabrication and processing levels of production are streamlined for limited productions runs (such as 10 fairings per month).

The frame, as presented, has a cost of $2437.18. Production costs would be expected to decrease when material is ordered in bulk and the manufacturing process is optimized for production. Optimization includes the construction of a more robust welding frame, dedicating notching jigs and potentially outsourcing some assembly processes such as wheel building. It would cost approximately $2,000 per frame for an annual production of 10 frames per month.

Table 15: Vehicle Cost for Production Run

Fairings	Cost Per Unit	Frames	Cost Per Unit
1	$2159.51	1	$2437.18
5	$1091.15	5	$2200
10	$957.61	10	$2000
120	$835.19	120	$1900

3. Testing

3.1 Frame Loading

Roll bar and frame integrity testing was done on the frame to ensure the safety of the rider in the event of a rollover. Load testing was done also to substantiate the results from the FEA and provide real-world results. The first case tested was top loading in which the frame was constrained at the dropouts and the front wheels/axle as shown in Figure 40. A **350-lbf** load was applied at the top of the roll bar in the downward direction, and this was mounted as shown in the figure. There was no significant deflection noted. This concurs with the FEA analysis which shows that the roll bar would only deflect 0.23 inches under a load of 485 lbf. With the results from the testing, it can be conjectured that under another 135 lbs, the roll bar would not deflect much. Further testing will verify this and discussed during the oral presentation of the design event.

The second test was side loading in which the frame was constrained at the front axle and the bottom of the frame. A **200-lbf** load was applied to the side of the frame at the position where the rider's head would be, as shown in Figure 40. No significant deflection was noted in the roll bar, which agrees the FEA which showed that under a 260-lbf load the deflection was 0.24 inches. The test results determined that with another 60 lbs, the roll bar would deflect very little. At the time of the test, the roll bar main tube did not yet have the additional side extensions for rider head width which it will have for the competition. This means that the roll bar will be even stiffer, and will be safe in the event of a rollover.

Figure 40: Roll bar Load Testing

3.2 Frame/Fairing Integration

Throughout the design phase, it became apparent that it was necessary to run physical tests to assure that our design ideas would work on a real vehicle. After careful analysis of the steering vibration problem of last year's vehicle, it was deduced that the issue circled around the frame/fairing connection. Last year's design included an adjustable crank boom arm, and due to this, the front half of the fairing was not supported, which resulted in a cantilever-type motion while driving. This motion was translated through the support rods and into the steering mechanism, making steering control very unstable. The design will have a stationary crank boom and feature an adjustable seat. Because of this, it was decided to include a support rod from the front of the frame to the bottom of the fairing. This concept was tested with a steel pipe, as shown in Figure 41. It proved to greatly reduce the vibration in the steering and increased steering control. Another design feature that will be implemented is bushings between the support rods and fairing to aid in damping and absorbing energy.

Figure 41: Support Rod Testing

3.3 Impact

The 2008 model fairing is constructed primarily from a single layer of Carbon Fiber/Kevlar hybrid fabric. For support, ribs have been placed at regular intervals. To ensure these materials are selected and used properly, impact, tensile and abrasion test experiments were completed. Furthermore, drag, cooling, streamline and human testing have been conducted. Impact testing was completed on samples of the following material combinations:

- Carbon/Kevlar Hybrid Fabric
- .125" x 1" high density foam sandwiched between Carbon/Kevlar and 8.7oz fiberglass
- 2mm Coremat® sandwiched between carbon/Kevlar and 8.7oz fiberglass

All samples were vacuum bagged against a flat steel plate at 15 in-Hg and used epoxy resin. Each sample was cut to 1" widths using a band saw with a guide jig for consistency. After impact, all sample layers were broken except for the carbon/Kevlar layer. Interestingly, the carbon/Kevlar fabric elastically deformed and sprung back to its original position. This characteristic is highly desirable for a non structural fairing as the surface skin can deflect without breaking and without showing signs of damage. Figure 42 shows the setup and samples for the tensile and impact tests.

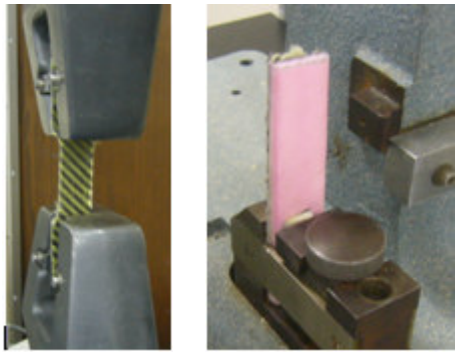

Figure 42: Left: Tensile Test; Right: Impact Test

The strongest of all samples tested is the Coremat® configuration. However, this strength comes at the price of weight. As Coremat® has a paper towel like absorption; it is rich in heavy resin making it nearly six times heavier than the foam rib configuration. Due to this weight, Coremat® was removed as a possibility for rib material.

3.4 Tensile

Samples were prepared to test the tensile strength of each sample. Foam ribs (.125" x 1") were vacuum bagged in two directions (in the direction of the Kevlar weave and in the direction of the Carbon weave). Additionally, carbon/Kevlar samples were also produced in the same fashion. To allow the tensile testing machine to clamp on the samples, metal plates were laid up between fiberglass and carbon/Kevlar to provide necessary thickness and rigidity. Finally, a 2mm Coremat® sample was made for comparison.

The stress strain curves in Figure 43 show tensile testing results, and Table 16 lists the fracture stresses for the samples. Names in parentheses indicate the axial load direction relative to the hybrid fabric. Notably, the foam samples have two fracture stresses. This occurred due to the layers present in the sample. The first peak, in both cases, represent where the carbon/Kevlar hybrid fracture while the second peak indicates where the foam/fiberglass layers fracture. The results of this show that the fiberglass is more ductile than the carbon/Kevlar, however both samples should be considered brittle materials. Further investigation with an optical microscope shows that when carbon fiber samples break, brittle shards are left behind as seen in Figure 44.

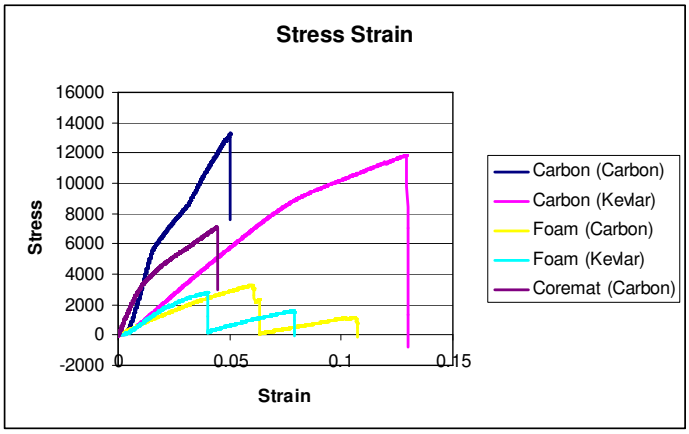

Figure 43: Stress-Strain Plot of Tensile Testing Results

Table 16: Fracture Stress

Sample (Orientation)	Fracture Stress (psi)
Foam Rib (Kevlar)	2799
Foam Rib (Carbon)	3267
No Rib (Kevlar)	11867
No Rib (Carbon)	13284

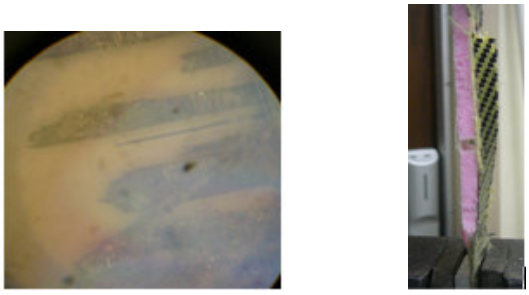

Figure 44: Left: Fractured Carbon Saw tooth (10x); Right: Sample after test

This fracture mode is significant for rider safety. Should the material break in this fashion, the rider will be exposed to a sharp edge. The solution for this problem is a layer of Kevlar laminated in areas where the rider may contact the fairing in a crash scenario.

3.5 Abrasion

In the unlikely event of a roll over, it is necessary to ensure the occupant is protected from road rash and from any broken composite material. An abrasion experiment was setup to subjectively observe the effects of dragging a loaded sample across concrete and asphalt. One of these two surfaces is likely to be the surface used for competition.

Samples were loaded with 50psi on a belt sander until destroyed. An 80 grit belt was used to represent an extreme worst case scenario road surface. The following samples were tested:

- Carbon/Kevlar
- Carbon/Kevlar with 1.7oz Kevlar inner layer
- Kevlar (1.7 oz)

Figure 45 shows the results of 120 seconds of loaded contact with the friction surface. The sample is shaved away and a generally smooth surface is left behind on the interior surface. Alone, the hybrid composite leaves a smooth interior with a rough and fuzzy exterior. This damage is not expected to injure the occupant; however the additional layer of Kevlar provides more abrasion resistance in the event of sliding crash.

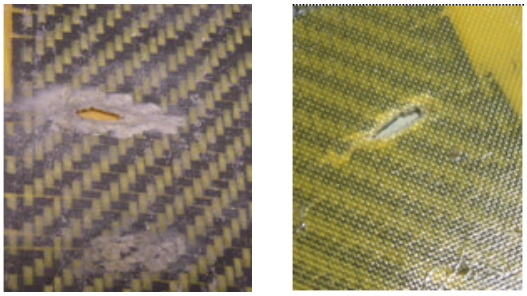

Figure 45: Hybrid (left) Hybrid with Kevlar (right)

3.6 Drag

For baseline testing, resistance data was collected. A nylon (no significant stretch) tether was attached to a digital fish scale which was secured to a hitch receiver on a team member's truck. The other end was attached to the 2007 HPV. Initially, the tether was 15 feet long. This effectively removed most wind resistance the HPV would otherwise experience. To calculate mechanical drag, the vehicle was towed behind the truck at a constant 10mph (slow speed for this test). The mechanical drag was measured to be 2.5lbf.

To measure aerodynamic drag, the tether was lengthened to 75 feet and the speed increased to 20mph (fastest speed the team considered safe for being connected to a truck). The drag was measured at 1lbf. This value was determined by subtracting mechanical resistance from the total resistance measured assuming negligible changes in mechanical drag with increased vehicle speeds.

Lastly, the hatch was removed. As a great deal of the endurance race was completed with the hatch off (due to high temperatures), it is noteworthy to measure the drag with the hatch removed. At 20mph, the aerodynamic drag is 4.5lbf. The frontal area remains constant due to the hatch geometry and location.

From these results, the teams determined that removing the hatch has a significant impact on aerodynamic performance. At the time of this report, the 2008 fairing was not completed sufficiently to do full scale, real world testing to compliment these baseline testing. Analytically, the aerodynamic drag was calculated to at 0.707lbf at 20mph. The analytical value for drag at 20mph is lower than the 2007 vehicle model. This is significant as the fairing shape is very different. The low weight expected from the materials selection compliments this streamlined shape.

3.7 Cooling

To determine the effectiveness of last year's submerged NACA ducts, each duct was subjectively tested independently. Each duct was taped shut and a rider pedaled the vehicle at cruising speed. The team found that ducts in the front of the vehicle are unnecessary as most air flow escapes through the front wheel cutouts. Additionally, the exit ducts were unnecessary. Sealing these rear exit ducts while leaving one entry duct directly in front of the

occupant's chest/face did not impede in the amount of mass airflow. Air easily escapes out of the vehicle through the cutout for the rear wheel.

3.8 Flow Visualization

To test for laminar flow, a 1/12 scale rapid prototype model was printed using the fused deposition modeling (FDM) technique. This model was mounted in a water tunnel with a dye injection system for flow visualization.

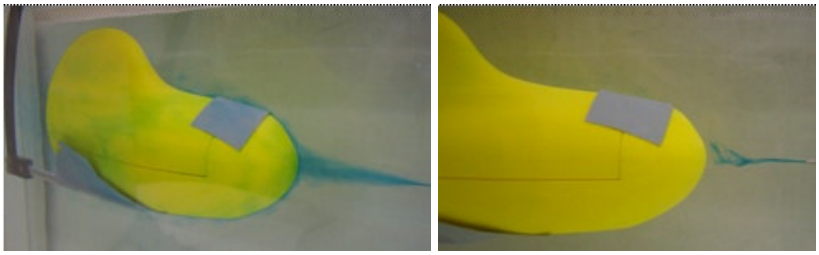

Figure 46: Left: Smoke Screen Right: High Pressure Stagnation

Figure 46 shows that flow over the body remains attached and laminar. Stagnation occurs in front of the nose cone. Figure 47 shows that flow separation is "clean," there are no eddies or swirls behind the vehicle.

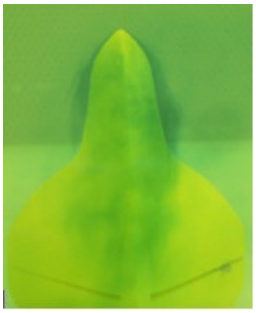

Figure 47: Rear view flow

Future testing for this model includes analysis in a subsonic wind tunnel to experimentally determine drag coefficient and pressure gradients over the vehicle. At the time of this report, the University wind tunnel was unavailable for use.

3.9 Rider Training Progress

At the heart of the event, performance is dependent on refined human power. Given a reliable vehicle with a suitable gear range, a team may be competitive in the sprint and endurance events if their human engine is in tune. The UCF human powered vehicle team consists of engineering students, most of which do not have any cycling background or recumbent cycling experience. To combat this issue, a training program was developed by a cycling/triathlon coach. The program encompasses speed and endurance training and diet has been taken into consideration. This program began in January of 2008 and ends a few days before the challenge.

To track improvement, bi-monthly power tests were conducted using a recumbent bike trainer available at the UCF's gym. The trainer can give average wattage output. Two wattage tests were conducted. First, a warm up followed by a one minute sprint and second, a 45 minute endurance (with an attempt to keep a sustained power output). Thus far, all members have shown improvement in power output, as shown in Figure 48.

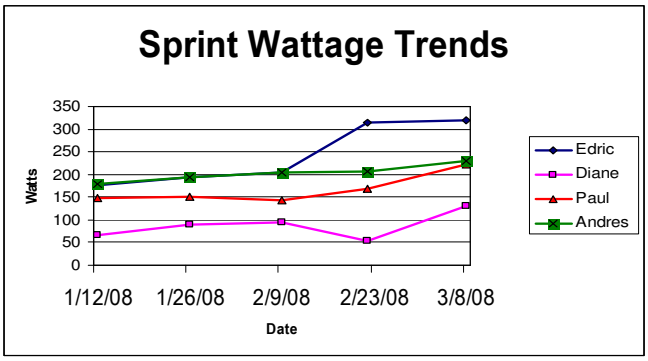

Figure 48: Wattage Progress Tracker

4. Safety

4.1 Frame Safety

For the UCF team, safety for the rider and spectators has always been paramount. For this reason, the team incorporated rollover protection and a safety harness and covered or deburred all sharp edges on the frame. The material of the frame is Chromoly steel which is a very safe and strong material. The roll bar is made of 1.5 inch outer diameter, 0.049 inch thick steel which provides excellent rollover and side protection for the rider.

All open holes have been covered with plastic or rubber end caps. Should the vehicle impact an object, no components are directly in front of the rider (such as a tiller steering mechanism common in two wheel configurations.) This eliminates the risk of rider to frame contact in a collision event even if the rider is not wearing his or her seatbelt. Clip pedals ensure that the rider's feet do not slip and get caught under the frame. Without these pedals and at high speeds, the rider is at risk of severe injury should his or her foot make contact with the road surface.

4.2 Fairing Safety

The fairing utilizes the vacuum bagging process will leave a smooth finish free of any sharp edges or potentially hazardous protrusions. In the event of a roll over where the vehicle slides on its side, the pilot is protected by a several mechanisms. Initial impact protection is provided by the frame's roll bar. However, the sliding motion typical of such accidents is managed by the outer skin of the fairing (hybrid carbon/Kevlar) in addition to a layer of Kevlar fabric in areas the pilot is likely to come in contact with (shoulders, arms, hips, etc.). This abrasion protection will prevent painful road rash injuries that are common of this type of crash. The fairing hatch may be opened from the outside to allow a team member to assist any sustained injury.

In the event of an impact with another vehicle or spectator, the fairing provides some protection for the third party. The outer skin of the fairing has excellent flexibility. Most impacts will cause the fairing to plastically deform requiring only light pressure to restore the original fairing shape. This deformation provides a protection boundary between internal components (chains, gears, pedals, etc.) and the unfortunate object being impacted. Again, the vacuum bag process provides a smooth surface such that the third party does not receive injuries due to sharp edges or blunt protrusions.

The best accident protection comes from accident prevention. A windscreen located close to the pilot's eyes allows for a larger field of vision with peripheral vision. This visibility increases the safety of the pilot and any pedestrians that may not be aware of the vehicle's presence. The fairing's dimensions allow for large steering changes resulting in a turning radius that exceeds the ASME requirements.

References

[1] Working Model 2005 Demo Version 8.0.1.0. *Design Simulation Technologies.* Canton, MI. 2006. Sept 2007 <http://www.workingmodel.com>.

[2] Brown, Sheldon. *Sheldon Brown's Gear Calculator*. 1998, 2008. 24 Nov 2007. <http://sheldonbrown.com/gears>.

[3] Locomotion <http://locomotionbikes.com/>.

[4] Zimmermann, Edward C. "Rambling about Cranks Lengths" *Basis Systeme netzwerk*. 24 Nov 2007 <http://www2.bsn.de/Cycling/cranks.html>.

[5] Fritzinger, Daniel. "The ins and outs of rack-and-pinion steering." *Dana Towing Group*. Albion, IN: 1 Mar 2001. 24 Nov 2008. <http://machinedesign.com/ContentItem/70954/Theinsandoutsofrackandpinionsteering.aspx>.

[6] Edgar, Julian. "Steering Angles". *Speed Pedal Human Powered Vehicles*. 2007. 24 Nov 2007. < http://www.speedpedal.com.au/cms/A_108424/title_Steering-Angles-/article.html>.

[7] Horwitz, Rickey M. "Trike Design 101 Part 1". *Hell-Bent Cycle Works*. Version 7.0. 24 Nov 2007. <http://www.hellbentcycles.com/Trike%20Design%20101%20%20part-1.htm>.

[8] Katz, Joseph, Ph.D. *Race Car Aerodynamics*, Cambridge Ma: Bentley Publisher, 2007.

[9] Wichers-Schreue, Ben. "The Ventilation of a Streamlined Human Powered Vehicles", *Abbot and Wilson*, 28 Jun 2004. 13 Nov 2007. <http://www.hupi.org/HPeJ/0002/ventilation2.pdf>.

[10] Mossman, Emmet A., Randall, Lauros M. "An Experimental Investigation of the Design: Variables for a NACA Submerged Duct Entrance", *National Advisory Committee for Aeronautics*, 8 Jan 1948. 11 Nov 2007. <http://naca.central.cranfield.ac.uk/reports/1948/naca-rm-a7i30.pdf>.

[11] Ashby, Michael F. *Materials Selection in Mechanical Design*. Oxford: Elsevier. 2005. 3rd Ed.

[12] *Matweb Material Property Data*. 1996-2008. 24 Nov 2007 <http://www.matweb.com>.

[13] SolidWorks 2007 Professional Edition. *SolidWorks Corporation*. Massachusetts Institute of Technology. 1995.